Springer

Journal of
Mechanical
Science and
Technology

Journal of Mechanical Science and Technology 22 (2008) 999~1007

www.springerlink.com/content/1738-494x

Multi-objective optimization of an axial compressor blade

Abdus Samad and Kwang-Yong Kim*

Department of Mechanical Engineering, Inha University, 253 Yonghyun-Dong, Nam-Gu, Incheon, 402-751, Rep. of Korea

(Manuscript Received January 26, 2007; Revised January 29, 2008; Accepted January 30, 2008)

Abstract

Numerical optimization with multiple objectives is carried out for design of an axial compressor blade. Two conflicting objectives, total pressure ratio and adiabatic efficiency, are optimized with three design variables concerning sweep, lean and skew of blade stacking line. Single objective optimizations have been also performed. At the data points generated by D-optimal design, the objectives are calculated by three-dimensional Reynolds-averaged Navier-Stokes analysis. A second-order polynomial based response surface model is generated, and the optimal point is searched by sequential quadratic programming method for single objective optimization. Elitist non-dominated sorting of genetic algorithm (NSGA-II) with ε-constraint local search strategy is used for multi-objective optimization. Both objective function values are found to be improved as compared to the reference one by multi-objective optimization. The flow analysis results show the mechanism for the improvement of blade performance.

Keywords: Compressor blade; Shape optimization; Genetic algorithm; Total pressure adiabatic efficiency

1. Introduction

Recently, several efforts have been made to improve the performance of turbomachinery blades by researchers applying optimization algorithms in assistance with the computational power replacing hit and trial approach and expensive experimental setup. Application of optimization methods has reduced the computational cost sharply for predicting the better design of turbomachines to enhance the performance in terms of reducing weight and flow loss, enhancing efficiency, pressure and surge margin, etc. by changing shape of stacking line, camber profile, etc.

The use of sweep, lean (dihedral), and skew (shifting stacking line in rotational direction) in an axial flow compressor rotor has become a matter of interest in the design of turbomachinery blades by many researchers [1-5]. These blade shape parameters, which form a three-dimensional stacking line, are generally introduced to reduce shock losses, corner separation in the blade hub, and tip clearance losses in transonic compressor rotors. Design of blade stacking line by using numerical optimization techniques has been reported by Jang et al. [6, 7], and Samad et al. [8]. These papers report the response surface approximation based optimization methods. The response surface method (RSM) [9], which is a global optimization method, was recently introduced as a tool of design optimization in turbomachinery. Different surrogate-based optimization models have been evaluated by Samad et al. [8] for design of compressor blade stacking line employing efficiency, total temperature and total pressure as single objectives.

Engineering design generally involves multiple disciplines and simultaneous optimization of multiple objectives related to each discipline. These design problems, which are usually known as multi-objective problems, require simul-taneous consideration of all objective functions to optimize the system. There are numbers of solution methods and algorithms available for solving multi-objective optimization problems [10-14]. In multi-objective optimizations of turbomachinery blades, efficiency, total pressure,

*Corresponding author. Tel.: +82 32 872 3096, Fax.: +82 32 868 1716
E-mail address: kykim@inha.ac.kr
DOI 10.1007/s12206-008-0122-5

static pressure, pressure loss, weight, stress, etc. are used as objectives, and variables related to camber profile and/or stacking line of blade are employed as design variables [15-18]. A multi-objective optimization problem consists of many optimal solutions called Pareto-optimal solutions; therefore, a designer's aim is to find as many optimal solutions as possible within the design range. This helps find a global Pareto-optimal front. Each design set corresponding to an optimal solution represents a compromise of design objectives. Elitist non-dominated sorting genetic algorithm (NSGA-II) given by Deb and Goel [19] generates Pareto-optimal solutions using an evolutionary algorithm. Goel et al. [20] presented ε-constraint strategy combined with NSGA-II algorithm using a polynomial-based response surface algorithm.

This work presents a multi-objective optimization procedure for design of a NASA rotor 37 [21] axial compressor blade. Multi-objective optimization by ε-constraint strategy [20] through NSGA-II algorithm [19] considering two conflicting objectives, i.e., total pressure ratio and adiabatic efficiency, and three design variables has been performed. For single objective optimization, a polynomial-based response surface approximation (RSA) model is used. Three-dimensional Reynolds averaged Navier-Stokes equations (RANS) are solved for internal flow analysis to evaluate the efficiency and total pressure ratio.

2. NASA rotor 37 and numerical analysis

A NASA rotor 37 [21], which is an axial-flow compressor rotor having a low-aspect ratio, is used for blade shape optimization. The detailed specifications of the compressor are summarized in Table 1. The rotor tip clearance is 0.356mm (0.45 percent span) and the measured choking mass flow rate is 20.93kg/s, which corresponds to 103.67% of the design flow rate. Total pressure, total temperature and the adiabatic efficiency in relation to the mass flow rates are measured at inlet and outlet positions. The inlet and outlet positions are located at 41.9mm upstream of the tip leading edge of the rotor and at 101.9mm downstream of the tip trailing edge of the rotor, respectively.

The three-dimensional thin-layer Navier-Stokes and energy equations are solved on body-fitted grids by using an explicit finite-difference scheme. An explicit Runge-Kutta scheme proposed by Jameson et al. [22] is used. Artificial dissipation terms have been added to resolve shocks. The algebraic turbulence model of Baldwin and Lomax [23] has been employed to estimate the eddy viscosity.

Table 1. Design specifications of NASA rotor 37.

Mass flow, kg/s	20.19
Rotational speed, rpm	17190
Pressure ratio	2.106
Inlet hub-tip ratio	0.70
Inlet tip relative Mach number	1.40
Inlet hub relative Mach number	1.13
Tip solidity	1.29
Rotor aspect ratio	1.19
Number of rotor blades	36

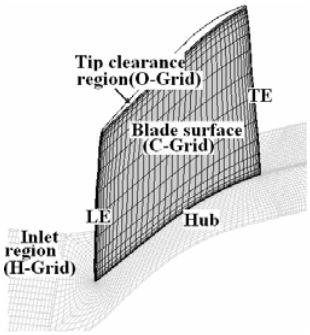

(a) Perspective view

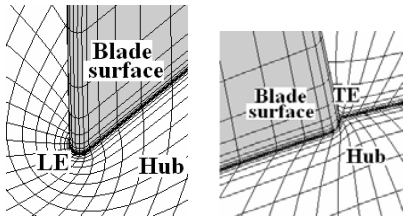

(b) Grids at hub of LE and TE

Fig. 1. Computational grids.

Fig. 1 shows the computational grids. A composite grid system with structured H-, C-, and O-type grids is adopted to represent the complicated configuration of the axial compressor. The H-type grid consists of 60×36×63 grids (in the streamwise, pitchwise and spanwise directions, respectively), and is introduced for the inlet flow region. The C-type grid consists of 350×46×63 grids, and is used for the blade passage. The O-type grid embedded in the tip clearance consists of 182×13×13 grids. The whole grid system has about 1,181,000 grids.

Mach numbers in each direction, total pressure and total temperature are given at the inlet. At the exit, the hub static pressure ratio has been specified and the radial equilibrium equation is solved along the blade span. A periodic tip clearance model is used to resolve the tip clearance flow explicitly. No-slip and adiabatic wall conditions are used at the wall boundaries. To reduce the computational load, the flow field in a single blade passage is simulated by applying a periodic boundary condition in the tangential direction.

3. Objective functions and design variables

The adiabatic efficiency (η_{ad}) and total pressure ratio (P_T) are selected as objective functions for the shape optimization of the rotor blade. The advantage of these objectives is the reduced weight and drag of the aircraft engine resulting in improved SFC (specific fuel consumption) for the gas turbine systems. In order to improve compressor blade performance, the objective functions are defined as:

$$\eta_{ad} = \frac{\left(P_{0exit}/P_{0inlet}\right)^{(k-1)/k} - 1}{T_{0exit}/T_{0inlet} - 1} \quad (1)$$

$$P_T = P_{0\,exit}/P_{0\,inlet} \quad (2)$$

where, k is ratio of specific heats, P_0 and T_0 are total pressure and total temperature, respectively. The goal of optimization is to maximize η_{ad} and P_T.

Three design variables are selected in these optimizations: one for sweep, one for lean, and the other for skew. Sweep is the movement of aerofoil sections of the blade in the direction of the chord line. Blade sweep, α, is defined as the displacement of the aerofoil in the axial direction at the rotor tip, and is normalized by the axial tip chord (= 27.77mm). The aerofoil sections are moved towards downstream direction for positive sweep (α). The line of the swept blade between the rotor tip and hub is linearly connected and tip clearance gap is kept constant.

Lean is the movement of aerofoil sections normal to the chord line. Blade lean, β, is defined as the displacement of airfoils normal to the chord line. Lean also is normalized by the axial tip chord. Here, lean, β is taken as positive if the aerofoil sections are moved towards the blade suction surface side. Lean (β) is taken as zero at the hub and linearly connected from hub to tip while tip clearance is kept constant.

Fig. 2 represents the skewed blade stacking line,

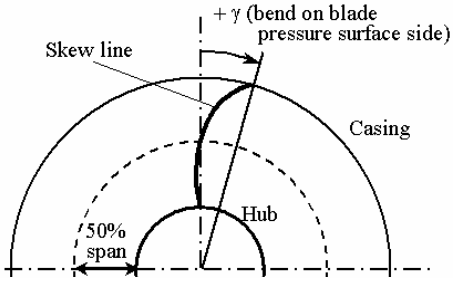

Fig. 2. Definition of blade skew (front view).

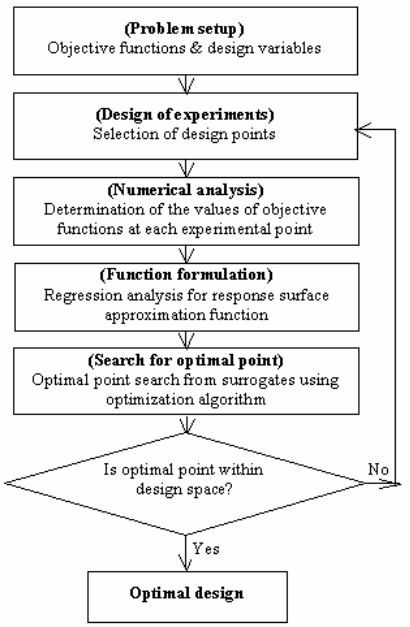

Fig. 3. Optimization procedure for single objective optimization.

and a single skew angle (γ) is defined only at the rotor tip. If the blade bends towards the pressure surface side, the skew angle is taken as positive. The skew line is defined by a second order polynomial. The constants and the coefficients are found by the constraints; skew angle is zero at both hub and mid span. The skew angle (γ) is set at tip of the blade.

4. Optimization methodology

Single and multi-objective optimization procedures which are followed in this paper are described in flowchart shown in Figs. 3 and 4, respectively. Initially, the variables are selected, and the design space is decided for improvement of system performance. The design points are selected by design of experiment (DOE), and the objective functions are cal culated

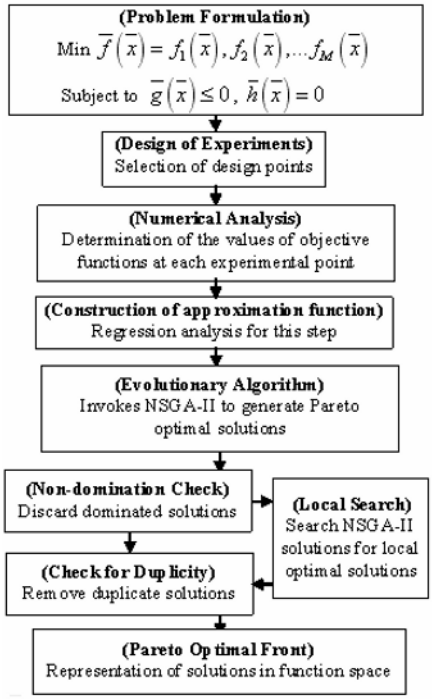

Fig. 4. Optimization procedure for NSGA-II

at these design points by using a flow solver. In this work, the DOE is conducted through a three-level fractional factorial design. Evaluations of the objective functions at these design points are performed by three-dimensional RANS analysis. These RANS analysis data are used to generate polynomial response surface functions for single as well as multi-objective optimization.

4.1 Single objective optimization

In single objective optimization, the CFD generated data are fitted on a curve to generate polynomial function. A second order polynomial-based response surface function (RSA) [10] is used to fit the data obtained from RANS analysis. In this method, if the regression coefficients are *β's,* the polynomial function becomes:

$$\hat{F} = \beta_0 + \sum_{j=1}^{n} \beta_j x_j + \sum_{j=1}^{n} \beta_{jj} x_j^2 + \sum \sum_{i \neq j}^{n} \beta_{ij} x_i x_j \qquad (3)$$

where *n* is number of design variables, and *x*'s are the design variables. Optimal point is searched by using sequential quadratic programming (SQP) [24] from the fitted curve.

4.2 Multi-objective optimization with NSGA-II

A multi-objective approach gives a set of optimal solutions instead of a single optimal solution. None of the solutions in this set of optimal solutions can be considered to be better than any other solution with respect to all objectives considered in the problem. These optimal solutions are Pareto-optimal solutions and their functional space representation is termed as Pareto-optimal front [14]. A number of methods are available [14] for solving multi-objective optimization problems, but the classical way of tackling a multi-objective problem is to convert it into a single objective problem. The methodology of constructing a global Pareto-optimal front is explored to get inside of the trade-off analysis between different conflicting objectives.

A multi-objective problem may be defined as:

Minimize $\bar{f}(\bar{x})$ (M function to be optimized)

Subject to $\bar{g}(\bar{x}) \le 0$ (m inequality constraints)

$\bar{h}(\bar{x}) = 0$ (p equality constraints)

where $\bar{f}(\bar{x}) = \{f_1(\bar{x}), f_2(\bar{x}), f_3(\bar{x}), \ldots\ldots f_M(\bar{x})\}$ is a vector of n real valued objective functions and *x* is a vector of *n* design variables. $\bar{x} \in R^n$, $\bar{g}(\bar{x}) \in R^m$, $\bar{h}(\bar{x}) \in R^p$. In general, engineering problems are associated with some conflicting objectives in which improvement of one objective leads to deterioration of others. Each feasible solution of the set $\bar{x}$ of a multi-objective problem is either a dominated or non-dominated solution, in which all non-dominated solutions are Pareto-optimal solutions. Vector $\bar{x}_i$ dominates a vector $\bar{x}_j$ if $\bar{x}_i$ is at least as good as $\bar{x}_j$ for all objectives and $\bar{x}_i$ is strictly better than $\bar{x}_j$ for at least one objective.

The methodology used to generate a global Pareto-optimal front is shown in Fig. 4. Objective functions and constraints are defined mathematically and evaluated on the data obtained from numerical experiments. A polynomial-based RSA model is constructed for the objective functions to reduce the complexity of the multi-objective optimization problem. A multi-objective evolutionary algorithm (MOEA) [14] is used to find Pareto-optimal solutions. The present study uses real coded NSGA-II [19].

The different parameters are adjusted one by one to suit the nature of the problem. Population size=100, Generation=250, Crossover=20, and Mutation =200.

NSGA-II gives a set of approximate Pareto-optimal solutions, and therefore an ε-constraint strategy [20] of the local search method is used to improve the quality of Pareto-optimal solutions. In ε-constrained strategy, one objective is taken as a constraint and the other is optimized by SQP. The step is repeated for each objective function over all the NSGA-II obtained solutions. These optimized solutions are merged with NSGA-II obtained solutions, and dominated solutions are discarded. The global Pareto-optimal solutions are achieved after duplicate solutions are removed from the non-dominated solutions.

5. Results and discussion

All computations reported in this paper to optimize blade shape are accomplished at design flow rate (20.19kgs^-1). Exit static to inlet total pressure ratio is set for each run of the program in the computer for each design point to fix the mass delivery rate at design flow condition. 0.2% fluctuations in design mass flow are allowed. Fig. 5 shows the validation of numerical results with experimental data [21] for the reference blade. The total pressure ratio and adiabatic efficiency are validated, and the little difference between the numerical and experimental result is due to numerical error. In the figure, the mass flow rates are normalized with the choking flow rate (20.93 kg/s).

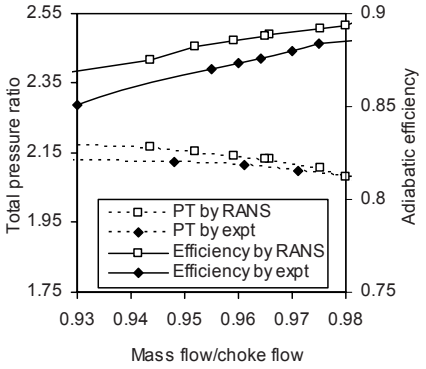

Fig. 5. Validation of RANS results with experimental data.

Table 2. Design variables and ranges.

Variables	Lower limit	Upper limit
Sweep (α)	-0.126	0.252
Lean (β)	-0.036	0.000
Skew (γ)	0.000	0.100

Ranges of the variables which constitute the design space for computations are decided by preliminary calculations. The design space is pre-sented in Table 2. Using this space, design points are generated by D-optimal design, and objective function values are computed by RANS analysis. At the next step, the objective function values are optimized by the statistical optimization models and their results are described in the following sections.

5.1 Single and multi-objective optimization

The problem for two objectives is handled by using single as well as multiobjective optimization. The Pareto-optimal front shown in Fig. 6 is obtained using NSGA-II with ε-constraint strategy for two objectives: total pressure ratio (P_T) and adiabatic efficiency (η_{ad}). From the figure, if one objective is maximized, the other objective value is reduced. The RANS analysis result for the reference blade is also shown in the figure. The single objective optimization for η_{ad} shows a gain in efficiency and a loss in P_T. Similarly, single objective optimization for P_T shows a gain in P_T and a loss in η_{ad}. The single objective optimizations show that the values of the objectives are located at extreme ends of the Pareto-optimal front. The Pareto-optimal front thus presents a choice to designers for choosing the objective function values according to their design needs. The RANS computed points are shown in this Fig. for these single objective optimizations. Since, NSGA-II is the compromise of these two objectives. Obviously, the Pareto curve shows an improvement of these objectives from the reference blade. To show the use of the Pareto curve, one point is randomly selected on the Pareto curve and computed by RANS analysis. The point is shown

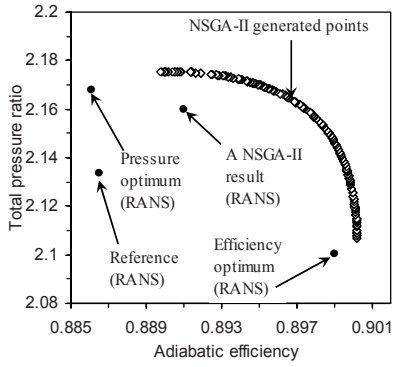

Fig. 6. Pareto-optimal design.

Table 3. Results of optimizations.

Objectives	Optimal points			RANS calculated Objective function					
				Values from optimal shape		Reference shape		% increased	
	α	β	γ (radians)	P_T	η_{ad}	P_T	η_{ad}	P_T	η_{ad}
P_T	-0.093	-0.007	0.017	2.168	0.886	2.133	0.887	1.62	-0.04
η_{ad}	0.102	-0.009	0.060	2.100	0.899			-1.55	1.41
A NSGA-II Multi-objective result	-0.019	-0.004	0.035	2.160	0.891			1.25	0.51

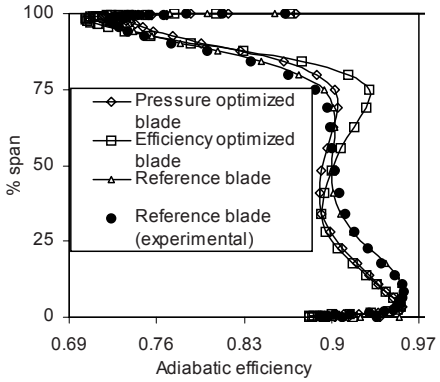

Fig. 7. Spanwise efficiency distributions.

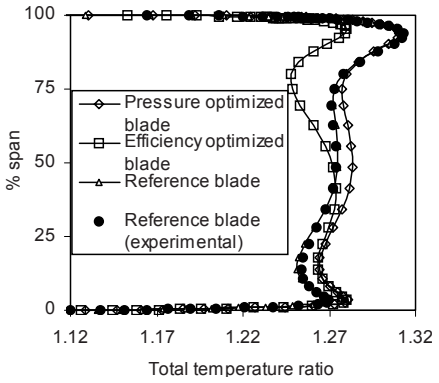

Fig. 8. Spanwise total temperature ratio distributions.

in the figure and the improvements of objectives are visible.

Table 3 shows the optimal design variables and the objective function values at these points. When only P_T is optimized, total pressure ratio is increased by 1.62%, while the efficiency is reduced by 0.04% in comparison with the reference blade. Similarly, if only efficiency is optimized as a single objective problem, the increase in efficiency is 1.41% and reduction in total pressure ratio is 1.55%. These two single objective optimizations clearly show that if one objective is optimized the other is reduced. In this table and on the Fig. 6, another point is selected randomly from NSGA-II results and computed by RANS analysis. The result shows the efficiency and total pressure ratio are increased by 0.51% and 1.25%, respectively. When the efficiency is optimized, the blade sweep (α) is positive, whereas when the total pressure ratio is optimized, α is negative.

Since the overall performance of a turbomachinery blade is not a function of a single objective, multi-objective optimization is the proper strategy for turbomachinery blade optimization. The Pareto-optimal solutions provide useful data for a designer who must select the final optimum design.

5.2 Flow analysis

From Fig. 6, it is seen that the single objectives give optimal points at extreme ends of the Pareto-optimal front. Hence, the following flow analyses have been performed for these two optimized blades as well as the reference blade for the purpose of comparison.

Figs. 7-10 show the spanwise distributions of adiabatic efficiency (η_{ad}), total temperature ratio (T_T), total pressure ratio (P_T), and Mach number, respectively, for the reference and the two optimum blades in comparison with the experimental results (Reid and Moore, 1978) for the reference blade. The computational results for the reference blade are found to agree well with the experimental results (Reid and Moore, 1978) throughout the span.

The η_{ad} in Fig. 7 is obtained by mass averaging the local values tangentially. The maximum difference of the local η_{ad} between the computational and experimental results at the design flow rate is less than 4 %. This figure shows the η_{ad} is largely increased near 75% span and reduced near 25% span when the efficiency is optimized. The pressure-optimized blade shows almost negligible change in efficiency all

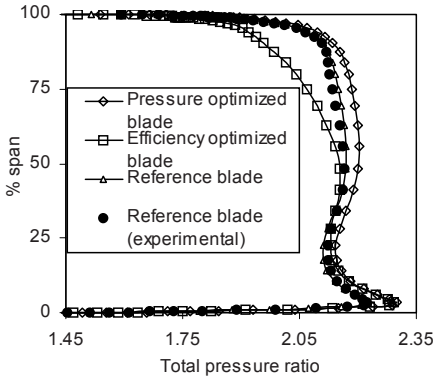

Fig. 9. Spanwise total pressure ratio distributions.

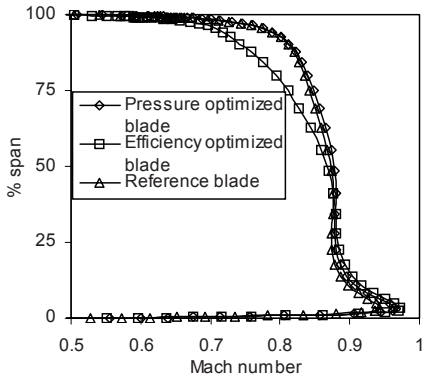

Fig. 10. Spanwise Mach number distributions.

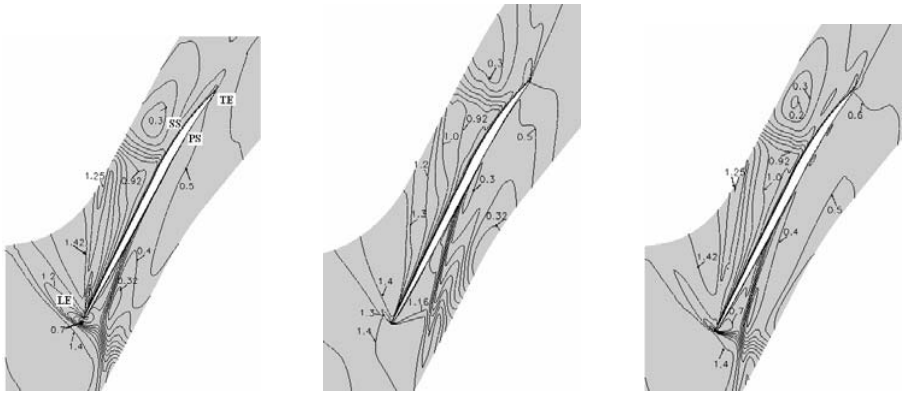

(a) Reference blade (b) Efficiency optimized blade (c) Total pressure ratio optimized blade

Fig. 11. Mach number contours at 80% span.

along the span.

Fig. 8 shows a significant reduction in total temperature ratio, $T_{T,}$ near the 75% span in the efficiency-optimized blade. Near the 10% span, the T_T is increased for both the pressure and the efficiency optimized blades.

Large reduction in P_T is observed near the 80% span when the blade is optimized for efficiency as shown in Fig. 9. On the other hand, the P_T is increased in the range from 25 to 80% span for the pressure-optimized blade.

Fig. 10 shows the Mach number distributions along the span. The reference and the pressure-optimized blades show almost the same results all along the span, while the efficiency-optimized blade shows a large reduction in Mach number near 80%.

In Fig. 11, Mach number distributions are shown for the reference (Fig. 11(a)) and two optimum blades (Fig. 11(b, c)) obtained from single objective optimizations. Mach number contours are drawn at 80% of span, where the Mach number is reduced largely by the efficiency-optimized blade in Fig. 10. It is clear that for the reference and the pressure-optimized blades, there is little change in Mach number profile. But, the efficiency-optimized blade (Fig. 11(b)) shows the separation line moved downstream. This movement of the separation line increases efficiency by reducing losses.

Fig. 12 shows the limiting streamlines on pressure and suction surfaces of the three blades. Separation lines are formed near the mid chord due to the interference between the passage shock and the suction surface boundary layer. Near the tip on the suction surface the separation lines moves largely downstream for the efficiency-optimized blade. This is consistent with the results shown in Fig. 7, where a relatively high increase in efficiency is observed near 75% span for the efficiency-optimized blade. An

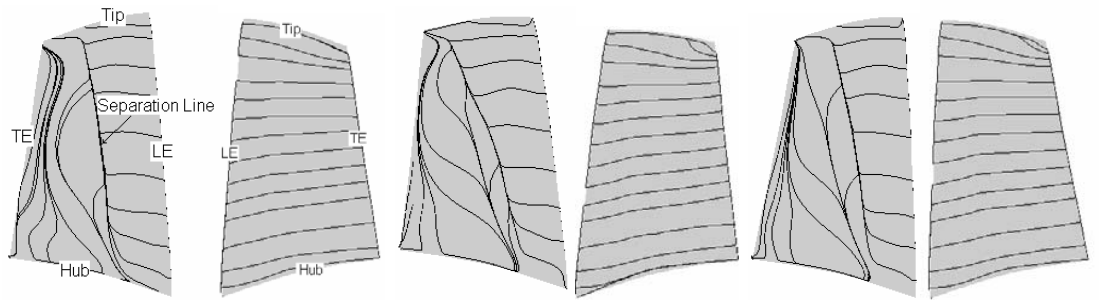

(a) Reference blade (b) Efficiency optimized blade (c) Pressure optimized blade

Suction surface Pressure surface Suction surface Pressure surface Suction surface Pressure surface

Fig. 12. Stream lines.

attachment line is also observed behind the separation line for all the three blades.

6. Conclusion

Single and multi-objective optimizations of a turbomachinery blade have been accomplished by using response surface approximation and ε-constraint NSGA-II algorithm coupling with RANS analysis, respectively. Two objectives, adiabatic efficiency and total pressure ratio, are optimized with three design variables concerning sweep, lean and skew of the blade stacking line. NSGA-II, which produces a Pareto-optimal front of conflicting objectives, produces compromised solutions which give enhanced results of both objectives. The single objective optimizations show that the values of the objectives are located at extreme ends of the Pareto-optimal front. Hence, the beauty of the multi-objective procedure is that it gives a set of solutions improving both objectives instead of giving a single solution obtained by single-objective optimization, which might affect other objectives or objectives not considered for optimization. Flow analysis results show that a large reduction in total pressure ratio is observed near the blade tip for the efficiency-optimized blade, while the total pressure ratio is increased in most of the spanwise region for the pressure-optimized blade. In the efficiency optimization, the efficiency is improved by shifting the separation line downstream on the suction surface near the tip of the blade.

Acknowledgments

The authors acknowledge the support from KISTI (Korea Institute of Science and Technology Information) under the Tenth Strategic Supercomputing Support Program, and Foreign Student Researcher Invitation Program of Korean Ministry of Science and Technology (KRF-2004-410052).

References

[1] S. J. Gallimore, J. J. Bolger and N. A. Cumpsty, The Use of Sweep and Diahedral in Multistage Axial Flow Compressor Blading, Part 1: University Research and Methods Development, Proceedings of ASME Turbo Expo,Amsterdam, The Netherlands, GT-2002-30328 (2002).

[2] J. D. Denton and L. Xu, The Effects of Lean and Sweep on Transonic Fan Performance, Proceedings of ASME Turbo Expo, Amsterdam, The Netherlands, GT-2002- 30327 (2002).

[3] N. Cai, J. Xu and A. Benaissa, Aerodynamic and Aeroacoustic Performance of a Skewed Rotor, Proceedings of ASME Turbo Expo, Atlanta, GA, GT-2003-38592 (2003).

[4] A. Fischer, W. Riess and J. Seume, Performance of Strongly Bowed Stators in a 4-Stage High Speed Compressor, Proceedings of ASME Turbo Expo, Atlanta, GA, GT-2003-38392 (2003).

[5] E. Benini and R. Biollo, On the Aerodynamics of Swept and Leaned Transonic Compressor Rotors, ASME Turbo Expo, Spain, GT2006-90547 (2006).

[6] C. M. Jang and K. Y. Kim, Optimization of a Stator Blade using Response Surface Method in a Single-Stage Transonic Axial Compressor, *Proceedings of The Institution of Mechanical Engineers, Part A – Journal of Power and Energy*, 219 (8) 595-603.

[7] C.-M. Jang, P. Li and K. Y. Kim, Optimization of Blade Sweep in a Transonic Axial Compressor

Rotor, *JSME International Journal-Series B*, 48 (4) (2005) 793-801.

[8] A. Samad, K. Y. Kim, T. Goel, R. T. Haftka and W. Shyy, Shape Optimization of Turbomachinery Blade using Multiple Surrogate Models, ASME Joint-U.S.-European Fluids Engineering Summer Meeting, FL, USA. FEDSM2006-98368 (2006).

[9] A. Messac, Physical programming: Effective optimization for computational design, *AIAA Journal*, 34 (1) (1996) 149-158.

[10] R. H. Myers and D. C. Montgomery, Response Surface Methodology: Process and Product Optimization using Designed Experiments, John Wiley & Sons, New York (1995).

[11] P. Sen and J.-B. Yang, Multiple criteria decision support in engineering design, London: Springer Verlag, New York (1998).

[12] K. Deb, S. Agrawal, A. Pratap and T. Meyarivan, A fast and elitist multi-objective genetic algorithm for multi-objective optimization: NSGA-II, Proceedings of the parallel problem solving from nature VI conference, Paris, 849-858 (2000).

[13] V. Chankong and Y. Y. Haimes, Multiobjective decision making theory and methodology, New York: Elsevier Science (1983).

[14] Y. Collette and P. Siarry, Multiobjective Optimization: Principles and Case Studies, New York, Springer (2003).

[15] L. Jun, L. Guojun, F. Zhenping and L. Lijun, Multiobjective optimization approach to turbomachinery Blades Design, ASME Turbo Expo, Nevada, USA. GT2005-68303 (2005).

[16] S. Obayashi, D. Sasaki and A. Oyama, Finding Tradeoffs by using Multiobjective Optimization Algorithms, *Transactions of JSASS*, 47 (155) (2004) 51-58.

[17] S. Obayashi, T. Tsukahara and T. Nakamura, Multiobjective Genetic Algorithm Applied to Aerodynamic Design of Cascade Airfoils, *IEEE Transactions on Industrial Electronics*, 47 (1) (2000) 211-216.

[18] E. Benini, Three-Dimensional Multi-Objective Design Optimization of a Transonic Compressor Rotor, *Journal of Propulsion and Power*, 20 (3) (2004) 559-565.

[19] K. Deb and T. Goel, Multi-objective evolutionary algorithms for engineering shape design, Evolutionary Optimization (Eds. R. Sarker, M. Mohammadin, X. Yao), Kluwer, 147-176 (2000).

[20] T. Goel, R. Vaidyanathan, R. T. Haftka and W. Shyy, Response surface approximation of Pareto-optimal front in multi-objective optimization, 10th AIAA/ISSMO Multidisciplinary Analysis and Optimization Conference, NY, USA. AIAA 2004-4501 (2004).

[21] L. Reid and R. D. Moore, Design and Overall Performance of Four Highly-Loaded, High-Speed Inlet Stages for an Advanced, High-Pressure-Ratio Core Compressor, NASA TP-1337 (1978).

[22] A. Jameson, W. Schmidt and E. Turkel, Numerical Solutions of the Euler Equation by Finite Volume Methods using Runge-Kutta Time Stepping Schemes, AIAA Paper No. 81-1259 (1981).

[23] B. S. Baldwin and H. Lomax, Thin Layer Approximation and Algebraic Model for Separated Turbulent Flow, AIAA Paper No. 78-257 (1978).

[24] MATLAB®, The language of technical computing, Release 14. 2004, The MathWorks Inc.